Journal of the Physical Society of Japan
Vol. 78, No. 8, August, 2009, 083703

Combined Approach of Density Functional Theory and Quantum Monte Carlo Method to Electron Correlation in Dilute Magnetic Semiconductors

Jun-ichiro OHE[1,2*], Yoshihiro TOMODA[1], Nejat BULUT[1,2], Ryotaro ARITA[3], Kazuma NAKAMURA[3], and Sadamichi MAEKAWA[1,2]

[1]*Institute for Materials Research, Tohoku University, Sendai 980-8577*
[2]*CREST, Japan Science and Technology Agency (JST), Kawaguchi, Saitama 332-0012*
[3]*Department of Applied Physics, University of Tokyo, Bunkyo, Tokyo 113-8656*

(Received May 12, 2009; accepted June 15, 2009; published July 27, 2009)

We present a realistic study for electronic and magnetic properties in dilute magnetic semiconductor (Ga,Mn)As. A multi-orbital Haldane–Anderson model parameterized by density-functional calculations is presented and solved with the Hirsch–Fye quantum Monte Carlo algorithm. Results well reproduce experimental results in the dilute limit. When the chemical potential is located between the top of the valence band and an impurity bound state, a long-range ferromagnetic correlations between the impurities, mediated by antiferromagnetic impurity–host couplings, are drastically developed. We observe an anisotropic character in local density of states at the impurity-bound-state energy, which is consistent with the STM measurements. The presented combined approach thus offers a firm starting point for realistic calculations of the various family of dilute magnetic semiconductors.

KEYWORDS: magnetic semiconductors, quantum Monte Carlo method, density functional theory
DOI: 10.1143/JPSJ.78.083703

The discovery of ferromagnetism in dilute magnetic semiconductor (DMS) materials, represented by a (Ga,Mn)-As system, has created much activity in the field of spintronics.[1–4] In the low-doping regime ($\ll 1\%$), (Ga,Mn)-As is insulating with a clear experimental evidence for the presence of an Mn-induced impurity band located at 110 meV above the valence band.[5] The position of the impurity level and the impurity-induced carriers are key quantities in generating the ferromagnetism. Various model studies[6–10] have clarified that this ferromagnetic correlations between the impurities are based on the polarization mechanism of the impurity-induced carriers.

However, it is still an open question whether this mechanism really works in real materials. In order to clarify this problem and step forward to the challenge for predicting new functional properties of the DMS materials and their realistic designs, many tasks such as nonempirical electronic-band structure of the host compound, reliable estimations for impurity–host hybridizations, and rigorous treatments for local electron correlations at the impurity site are required. A combined approach of density functional theory (DFT)[11] and quantum Monte Carlo (QMC) technique[12] is clearly useful for this purpose. The hybridization or mixing parameters between the host and impurity orbitals is a crucial parameter characterizing material differences and therefore this parameter should be estimated on the basis of *ab initio* density-functional calculations. On the other hand, density-functional calculations often fail to describe local electron correlations, so this problem must be treated with more accurate solvers such as the QMC technique. Critical comparisons with the experimental data are needed for a check whether this approach is really reliable in describing the details of the "low-energy" electronic and magnetic properties and/or whether it has an extended applicability for many DMS materials.

*E-mail: johe@imr.tohoku.ac.jp

In this letter, we present a comprehensive study for the generation mechanism of the ferromagnetism of a dilute (Ga,Mn)As system. A multi-orbital Haldane–Anderson model[13] is employed to describe electronic/magnetic properties of this system. First principles band-structure calculations are performed to evaluate the mixing matrix elements in this model and the resulting model is solved with the help of the QMC technique to examine the inter-impurity and impurity–host magnetic correlations. The hybridization between host and impurity electrons generates the impurity bound state.[14] When the chemical potential is located between the impurity bound state and the valence-band top, a notable long-range ferromagnetic correlation between the impurities and its dramatic enhancement as the temperature decreases are observed. We will show that this ferromagnetic correlation is mediated by antiferromagnetic impurity–host couplings. In addition, our calculated host local density of states is highly anisotropic around the impurity sites, which is also consistent with the experimental STM image.[15] These quantitative agreements with the experiments indicates that the presented combination idea is a useful approach for aiming at realistic calculations and searching new functional high-T_c DMS materials.

A multi-orbital Haldane–Anderson model is given as follows:[13]

$$\mathcal{H} = \sum_{\mathbf{k},\alpha,\sigma} (\epsilon_{\mathbf{k}\alpha} - \mu) c^{\sigma\dagger}_{\mathbf{k}\alpha} c^{\sigma}_{\mathbf{k}\alpha} + \sum_{i,\xi,\sigma} (E_{d\xi} - \mu) d^{\sigma\dagger}_{i\xi} d^{\sigma}_{i\xi} + \sum_{\mathbf{k},\alpha,i,\xi,\sigma} (V_{\mathbf{k}\alpha,i\xi} c^{\sigma\dagger}_{\mathbf{k}\alpha} d^{\sigma}_{i\xi} + \text{h.c.}) + U \sum_{i,\xi} d^{\uparrow\dagger}_{i\xi} d^{\uparrow}_{i\xi} d^{\downarrow\dagger}_{i\xi} d^{\downarrow}_{i\xi}. \quad (1)$$

Here, $c^{\sigma\dagger}_{\mathbf{k}\alpha}$ ($c^{\sigma}_{\mathbf{k}\alpha}$) creates (annihilates) a host electron with wavevector $\mathbf{k}$ and spin σ in the valence or conduction bands denoted by α, and $d^{\sigma\dagger}_{i\xi}$ ($d^{\sigma}_{i\xi}$) is a creation (annihilation) operator for a localized electron at impurity d orbital ξ located at transition-metal site i. The first term in eq. (1) represents a kinetic energy $\epsilon_{\mathbf{k}\alpha}$ of a host $\mathbf{k}\alpha$ electron, and the second term describes a bare onsite energy $E_{d\xi}$ of the

impurity and μ is a chemical potential. The third term specifies impurity–host hybridization $V_{\mathbf{k}\alpha,i\xi}$ and the last term represents the onsite repulsion U at the impurity site. In the present study, we keep only diagonal terms in the onsite interaction by neglecting the off diagonal terms in the interaction (i.e., Hund's rule coupling).

When a Mn atom is substituted in place of a Ga site, the five $3d$ orbitals of the Mn ion are split into the three-fold degenerate t_{2g} orbitals and the two-fold degenerate e_g orbitals by the tetrahedral crystal field. In the present Mn^{2+} case with a $3d^5$ configuration, the e_g orbitals are fully occupied and therefore are inactive for the magnetic properties. In contrast, the three-fold t_{2g} orbitals being a partially-filled state are active for the low-energy magnetic excitations.

The onsite repulsion was set to $U = 4.0\,\mathrm{eV}$ following a photoemission spectrum[16] and this value is very close to theoretical values $4-5\,\mathrm{eV}$ for metallic Mn.[17] Bare onsite energy $E_{d\xi}$ in eq. (1) is not the diagonal element of the hybridization matrix obtained from density functional calculation, because the latter already includes the correlation effect through the exchange correlation potential. If we set the diagonal element of the density functional hybridization matrix to $E_{d\xi}$ in the model Hamiltonian, the correlation effect is doubly counted at the stage solving the model with QMC. Thus, we adjust the value of $E_{d\xi}$ in order to avoid this double counting. The value was determined as follows: Experimentally, it is widely agreed that an impurity band exists in the dilute limit of (Ga,Mn)As at 110 meV above the valence band.[5] To realize this situation, we found that $E_{d\xi}$ should be set to $-2.0\,\mathrm{eV}$. The energy of the impurity bound state is shifted by 0.01 eV, when we changes the $E_{d\xi}$ by 0.1 eV.

Estimations for the hybridization parameters $V_{\mathbf{k}\alpha,i\xi}$ in eq. (1) need careful treatments. Empirical estimations with the Slater–Koster table fail to describe the dispersion of the conduction bands, thus leading to a serious failure in the hybridization-parameter estimation. We estimate the hybridization parameter $V_{\mathbf{k}\alpha,i\xi}$ in eq. (1) from *ab initio* density-functional calculations.[18] The matrix element is given by

$$V_{\mathbf{k}\alpha,i\xi} = \langle\psi_{\mathbf{k}\alpha}|\mathcal{H}_0|\varphi_{i\xi}\rangle, \tag{2}$$

where $\mathcal{H}_0$ is the one-body part of eq. (1), $|\psi_{\mathbf{k}\alpha}\rangle = c^{\sigma\dagger}_{\mathbf{k}\alpha}|0\rangle$, and $|\varphi_{i\xi}\rangle = d^{\sigma\dagger}_{i\xi}|0\rangle$. $|\psi_{\mathbf{k}\alpha}\rangle$ can be expressed with a linear combination of Wannier functions as

$$|\psi_{\mathbf{k}\alpha}\rangle = \frac{1}{\sqrt{N}}\sum_{\mu}\sum_{\mathbf{R}} a_{\alpha\mu}(\boldsymbol{k})\mathrm{e}^{\mathrm{i}\mathbf{k}\mathbf{R}}|w_{\mathbf{R}\mu}\rangle, \tag{3}$$

where $|w_{\mathbf{R}\mu}\rangle$ is the Wannier orbital at the lattice $\mathbf{R}$ and the label μ specifies the type of the orbitals. In the present GaAs case, the μ specifies the four types of sp^3 orbitals centered at a Ga or As site. Expansion coefficients $\{a_{\alpha\mu}(\boldsymbol{k})\}$ are obtained from solving the equation $\mathcal{H}_{cry}|\psi_{\mathbf{k}\alpha}\rangle = \epsilon_{\mathbf{k}\alpha}|\psi_{\mathbf{k}\alpha}\rangle$. By substituting eq. (3) into eq. (2), we obtain the form of

$$V_{\mathbf{k}\alpha,i\xi} = \frac{1}{\sqrt{N}}\sum_{\mu}\sum_{\mathbf{R}} a^*_{\alpha\mu}(\boldsymbol{k})\mathrm{e}^{-\mathrm{i}\mathbf{k}\mathbf{R}}\langle w_{\mathbf{R}\mu}|\mathcal{H}_0|\varphi_{i\xi}\rangle. \tag{4}$$

For an actual evaluation of the matrix element $\langle w_{\mathbf{R}\mu}|\mathcal{H}_0|\varphi_{i\xi}\rangle$, we utilize a supercell calculation: We first arrange a supercell containing $3\times3\times3$ fcc primitive cells, where a Ga atom located at the origin in the supercell is replaced with an Mn atom. We then make maximally localized Wannier functions[19] for this system.[20] Supercell Wannier functions were constructed with a $5\times5\times5$ k-points sampling. The width of an energy window was set in order to include all the valence-bonding and conduction-anti-bonding states. The total number of the resulting Wannier functions are 217 in which there are 212 GaAs Wannier orbitals $\{|w_{n\mu}\rangle\}$ with μ and n specifying four types of the sp^3 orbitals and sites of Ga or As, respectively, and five Mn-$3d$ Wannier orbitals $\{|w_{i\xi}\rangle\}$ sitting on the origin site i. Then, we calculate the matrix element $\langle w_{n\mu}|\mathcal{H}^{3\times3\times3}_{KS}|w_{i\xi}\rangle$ with $\mathcal{H}^{3\times3\times3}_{KS}$ being the Kohn-Sham Hamiltonian for the supercell. This matrix element is used instead of $\langle w_{\mathbf{R}\mu}|\mathcal{H}_0|\varphi_{i\xi}\rangle$ in eq. (4) for $\mathbf{R} \neq i$. We note that the error due to this replacement is scaled by $(1/M)$ with M being the total number of the atoms in the supercell. For $\mathbf{R} = i$, $\langle w_{\mathbf{R}\mu}|\mathcal{H}_0|\varphi_{i\xi}\rangle$ is expected to be negligibly small, since wave-function symmetry of $|w_{\mathbf{R}\mu}\rangle$ and $|\varphi_{i\xi}\rangle$ are different. We found that the hybridization parameters are rather short-ranged; these are nearly zero except for the nearest and next-nearest sites; for example, the parameters between the Mn-t_{2g} orbitals and the nearest As-sp^3 orbitals are $0.16-0.74\,\mathrm{eV}$, while the values between the t_{2g} orbitals and the next-nearest Ga-sp^3 orbitals are $0.06-0.14\,\mathrm{eV}$. Notice that, if the empirical Slater–Koster estimation is employed, the latter next-nearest values are zero. We neglect the spin–orbit interaction in the present paper, because the spin–orbit interaction is enough small ($\sim$0.1 eV) compared with the band width ($\sim$10 eV).

We perform the quantum Monte Carlo simulation for a one- or two-impurity Haldane–Anderson models, in which we use the Hirsch–Fye QMC algorithm[12] for obtaining the electronic correlations in the one- and two-impurity Haldane–Anderson models. In particular, we study with QMC the magnetic correlations and the local density of states around the impurity site. We define the magnetization operator at the ξ orbital of the i'th impurity site as $M^z_{i\xi} = n_{i\xi\uparrow} - n_{i\xi\downarrow}$, and at site $\mathbf{r}$ of the host as $m^z(\mathbf{r}) = n_\uparrow(\mathbf{r}) - n_\downarrow(\mathbf{r})$. Here, $n_{i\xi\sigma}$ and $n_\sigma(\mathbf{r})$ are the spin-dependent number operators at the impurity and host sites, respectively. For the single-impurity case, we present data on the average value of the square of the local moment at the impurity site, $\langle(M^z)^2\rangle = (1/3)\sum_{\xi=1}^{3}\langle(M^z_{i\xi})^2\rangle$, where ξ sums over the t_{2g} orbitals, while for the two-impurity case we show data on the magnetic correlation function defined by $\langle M^z_1 M^z_2\rangle = (1/3)\sum_{\xi=1}^{3}\langle M^z_{1\xi}M^z_{2\xi}\rangle$ for impurities located at sites $\mathbf{R}_1$ and $\mathbf{R}_2$. In the single-impurity case, we will also present data on the impurity–host magnetic correlation function, $\langle M^z m^z(\mathbf{r})\rangle = (1/3)\sum_{\xi=1}^{3}\langle M^z_{0\xi}m^z(\mathbf{r})\rangle$, where $\mathbf{r}$ is the host site and the impurity is located at the origin.

Figure 1 shows the square of the impurity magnetic moment $\langle(M^z)^2\rangle$ as a function of the chemical potential μ at various temperatures T for the single-impurity Anderson model. With decreasing T, we observe that a step-like discontinuity develops centered at $\mu \approx 0.1\,\mathrm{eV}$, which indicates that the impurity bound state is located at this energy.[10] Within the Hartree–Fock picture,[6,10] the impurity–host hybridization creates both the impurity bound state (IBS) and the host split-off state at ω_{IBS}. For $\mu < \omega_{\mathrm{IBS}}$, the hybridization with the valence band reduces the impurity magnetic moment. When μ is increased to above ω_{IBS}, the polarization of the split-off state cancels the polarization of

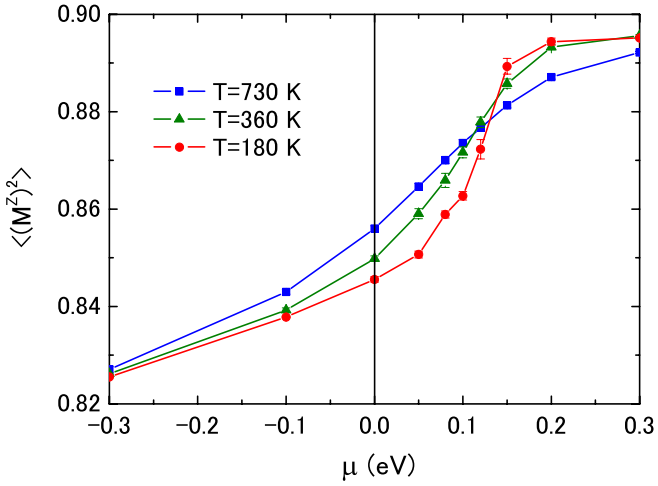

Fig. 1. (Color online) Square of the impurity magnetic moment $\langle (M^z)^2 \rangle$ vs the chemical potential μ at various temperatures in the single-impurity case. These results are for the single-impurity Haldane–Anderson model. The vertical line ($\mu = 0$) denotes the top of the valence band.

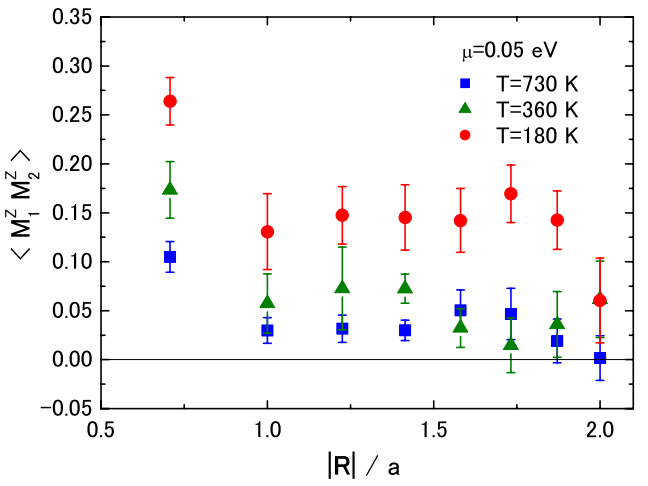

Fig. 2. (Color online) Inter-impurity magnetic correlation function $\langle M_1^z M_2^z \rangle$ vs the impurity separation $|\mathbf{R}|/a$ at various temperatures for μ fixed at 0.05 eV.

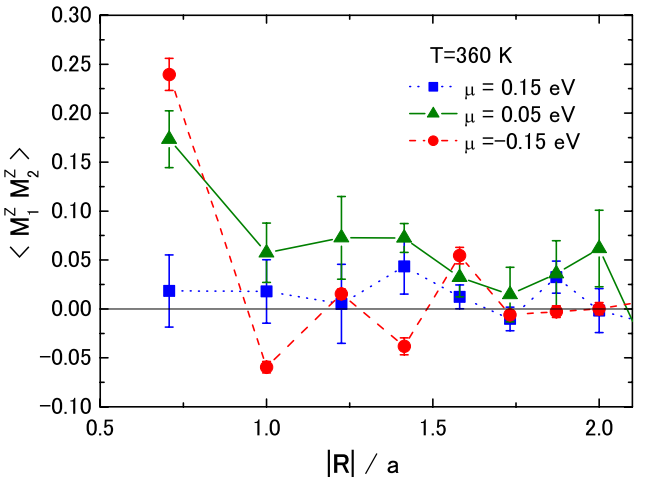

Fig. 3. (Color online) $\langle M_1^z M_2^z \rangle$ vs $|\mathbf{R}|/a$ at $T = 360$ K for various values of μ.

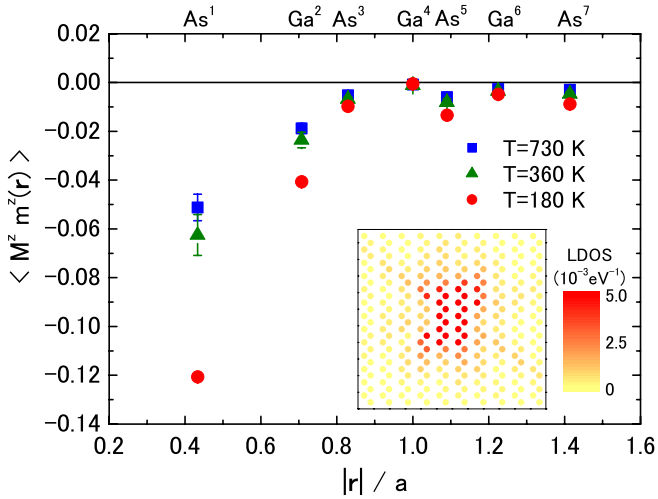

Fig. 4. (Color online) Impurity–host magnetic correlation function $\langle M^z m^z(\mathbf{r}) \rangle$ vs $|\mathbf{r}|/a$ for $\mu = 0.05$ eV and various temperatures in the single-impurity case. (Inset) Local density of states of the host electrons in the (011) plane. Here, the impurity is located at the next layer, and the circles indicate the position of the Ga and As sites. The size of this figure is $5 \times 5.6\,\mathrm{nm}^2$, and these results are for $T = 360$ K and $\mu = 0.05$ eV.

the valence band, which in turn decreases the screening of the impurity moment. This is the reason for why $\langle (M^z)^2 \rangle$ increases at ω_{IBS}.

Figure 2 shows the impurity–impurity magnetic correlation function $\langle M_1^z M_2^z \rangle$ vs $|\mathbf{R}|/a$ at various T for the two-impurity Anderson model. Here, $|\mathbf{R}| = |\mathbf{R}_1 - \mathbf{R}_2|$ is the impurity separation and a is the GaAs lattice constant. In addition, μ is fixed at 0.05 eV so that it is located between the top of the valence band and the impurity bound state. In Fig. 2, we observe that the ferromagnetic correlations become stronger and extended in real space, as T decreases down to 180 K, which is in the physically relevant temperature regime for (Ga,Mn)As.[2] We observe the ferromagnetic correlation within the 8th neighbors site at lowest temperature. The average concentration is 1.45% that is a low-doping regime. Figure 3 shows $\langle M_1^z M_2^z \rangle$ vs $|\mathbf{R}|/a$ at 360 K for $\mu = -0.15,\ 0.05,\ 0.15$ eV. For $\mu = -0.15$ eV, the chemical potential is located in the valence band. In this case, the system is metallic and we observe Ruderman–Kittel–Kasuya–Yosida (RKKY) type oscillations in the magnetic correlations. The ferromagnetic coupling disappears for $\mu = 0.15$ eV, where the impurity bound state becomes occupied. These results indicate that the chemical potential should be located between the impurity bound state and the valence band for obtaining extended ferromagnetic coupling between the impurity moments. This case corresponds to the insulating state of (Ga,Mn)As found in the dilute limit.[5] In addition, the strong μ, R and T dependence of $\langle M_1^z M_2^z \rangle$ observed in Figs. 2 and 3 makes it difficult to determine *phenomenologically* the magnetic coupling in DMS materials, instead requiring approaches which treat the band structure and correlation effect on an equal footing and exactly such as the DFT+QMC method used here.

In order to determine the origin of the ferromagnetic correlation between the impurities, we present in Fig. 4 the impurity–host magnetic correlation function $\langle M^z m^z(\mathbf{r}) \rangle$ vs $|\mathbf{r}|/a$ at various T for the single-impurity Haldane–Anderson model. These results are for $\mu = 0.05$ eV in which case the inter-impurity ferromagnetic correlation is strong. We

observe that the impurity–host magnetic coupling is anti-ferromagnetic and it enhances with decreasing temperature. When the impurity bound state is occupied ($\mu = 0.15\,\mathrm{eV}$), we find that the impurity–host anti-ferromagnetic magnetic coupling becomes much weaker (not shown here) and the inter-impurity ferromagnetic correlations collapse. Hence, the anti-ferromagnetic impurity–host coupling generates the indirect ferromagnetic coupling between the impurities.

Finally, in the inset of Fig. 4, we show local density of states around the Mn site defined by $N(\mathbf{r}) = -\mathrm{d}/\mathrm{d}\mu\langle n(\mathbf{r}) - n(\infty)\rangle|_{\mu=0.05\,\mathrm{eV}}$, where $n(\mathbf{r})$ is the electron number operator at site $\mathbf{r}$. The highly anisotropic distribution of local density of states around Mn is consistent with the STM measurements,[15,21] which again emphasizes the necessity of including both the band structure and correlation effect.[22,23] The anisotropy of local density of state is originated from the anisotropic mixing energy $V_{\mathbf{k}\alpha,i\xi}$ in eq. (1). We note that we observe the anistropy of the local density of state even without the spin–orbit interation in contrast to ref. 22.

In summary, we have investigated the magnetic properties of the dilute magnetic semiconductors (Ga,Mn)As in the dilute limit within a combined approach of the density functional theory and the quantum Monte Carlo method. For this purpose, we have mapped the electronic state of the system to the multi-orbital Haldane–Anderson model by using the density functional theory with maximally-localized Wannier functions. For calculating the magnetic properties, we have used the Hirsch–Fye quantum Monte Carlo method, which does not exhibit a fermion sign problem. Within this approach, we have correctly reproduced the experimental value for the energy of the impurity band of (Ga,Mn)As in the dilute limit. The numerical results emphasize the role of the impurity bound state in producing the ferromagnetic correlations. We have found that, when the chemical potential is between the top of the valence band and the impurity bound state, the inter-impurity ferromagnetic correlation originating from the anti-ferromagnetic impurity–host coupling is strong and extended in real space. This case corresponds to the insulating state found in the low-doping regime of (Ga,Mn)As. In addition, we have observed a highly anisotropic distribution of local density of states around Mn which is consistent with the STM measurements. The agreements found with the experimental data on the dilute limit of (Ga,Mn)As suggest that the proposed approach is a reliable method for investigating and designing other DMS materials. To investigate the Curie temperature, we should treat the system which has many impurities at lower temperature. It requires a huge amount of computer resources and it remains in future works.

Acknowledgments

We thank H. Ohno and M. E. Flatté for valuable discussions. This work was supported by the NAREGI Nanoscience Project and a Grant-in-Aid for Scientific Research from the Ministry of Education, Culture, Sports, Science and Technology of Japan. We thank the Supercomputer Center, Institute for Solid State Physics, University of Tokyo for the use of facilities.

1) *Concepts in Spin Electronics*, ed. S. Maekawa: (Oxford University Press, Oxford, U.K., 2006).
2) H. Ohno, H. Munekata, T. Penney, S. von Molnar, and L. L. Chang: Phys. Rev. Lett. **68** (1992) 2664; H. Ohno, A. Shen, F. Matsukura, A. Oiwa, A. End, S. Katsumoto, and Y. Iye: Appl. Phys. Lett. **69** (1996) 363.
3) I. Žutić, J. Fabian, and S. Das Sarma: Rev. Mod. Phys. **76** (2004) 323.
4) T. Jungwirth, J. Sinova, J. Masek, J. Kucera, and A. H. MacDonald: Rev. Mod. Phys. **78** (2006) 809.
5) T. Jungwirth, J. Sinova, A. H. MacDonald, B. L. Gallagher, V. Novak, K. W. Edmonds, A. W. Rushforth, R. P. Campion, C. T. Foxon, L. Eaves, E. Olejnik, J. Masek, S. R. Eric. Yang, J. Wunderlich, C. Gould, L. W. Molenkamp, T. Dietl, and H. Ohno: Phys. Rev. B **76** (2007) 125206.
6) M. Ichimura, K. Tanikawa, S. Takahashi, G. Baskaran, and S. Maekawa: *Foundations of Quantum Mechanics in the Light of New Technology (ISOM-Tokyo 2005)* (World Scientific, Singapore, 2006) pp. 183–186; cond-mat/0701736.
7) P. M. Krstajić, V. A. Ivanov, F. M. Peeters, V. Fleurov, and K. Kikoin: Europhys. Lett. **61** (2003) 235.
8) K. Yamauchi, H. Maebashi, and H. Katayama-Yoshida: J. Phys. Soc. Jpn. **72** (2003) 2029.
9) J. Inoue, S. Nonoyama, and H. Itoh: Phys. Rev. Lett. **85** (2000) 4610.
10) N. Bulut, K. Tanikawa, S. Takahashi, and S. Maekawa: Phys. Rev. B **76** (2007) 045220.
11) P. Hohenberg and W. Kohn: Phys. Rev. **136** (1964) B864; W. Kohn and L. J. Sham: Phys. Rev. **140** (1965) A1133.
12) J. E. Hirsch and R. M. Fye: Phys. Rev. Lett. **56** (1986) 2521.
13) F. D. M. Haldane and P. W. Anderson: Phys. Rev. B **13** (1976) 2553.
14) J. S. Blakemore, W. J. Brown, M. L. Stass, and D. A. Woodbury: J. Appl. Phys. **44** (1973) 3352.
15) A. M. Yakunin, A. Yu. Silov, P. M. Koenraad, J. H. Wolter, W. Van Roy, J. De Boeck, J.-M. Tang, and M. E. Flatté: Phys. Rev. Lett. **92** (2004) 216806.
16) J. Okabayashi, A. Kimura, O. Rader, T. Mizokawa, A. Fujimori, T. Hayashi, and M. Tanaka: Phys. Rev. B **58** (1998) R4211.
17) F. Aryasetiawan, K. Karlsson, O. Jepsen, and U. Schonberger: Phys. Rev. B **74** (2006) 125106.
18) *Tokyo Ab initio Program Package* is used for band calculations, within the generalized gradient approximation to the exchange correlation functional, using a plane-wave basis set and norm-conserving pseudopotentials. The energy cutoff is set to 49 Ry. For details for this code, see J. Yamauchi, M. Tsukada, S. Watanabe, and O. Sugino: Phys. Rev. B **54** (1996) 5586.
19) N. Marzari and D. Vanderbilt: Phys. Rev. B **56** (1997) 12847; I. Souza, N. Marzari, and D. Vanderbilt: Phys. Rev. B **65** (2001) 035109.
20) J. Okabayashi, A. Kimura, O. Rader, T. Mizokawa, A. Fujimori, T. Hayashi, and M. Tanaka: Phys. Rev. B **64** (2001) 125304.
21) C. Çelebi, P. M. Koenraad, A. Yu. Silov, W. Van Roy, A. M. Monakhov, J.-M. Tang, and M. E. Flatté: Phys. Rev. B **77** (2008) 075328.
22) J.-M. Tang and M. E. Flatté: Phys. Rev. Lett. **92** (2004) 047201.
23) G. A. Fiete, G. Zaránd, K. Damle, and C. P. Moca: Phys. Rev. B **72** (2005) 045212.